

Molecular Imaging of *bcl-2* Expression in Small Lymphocytic Lymphoma Using ^{111}In -Labeled PNA–Peptide Conjugates

Fang Jia¹, Said Daibes Figueroa², Fabio Gallazzi³, Baghavathy S. Balaji¹, Mark Hannink⁴, Susan Z. Lever⁵, Timothy J. Hoffman^{2,6}, and Michael R. Lewis^{1,2,7,8}

¹Department of Veterinary Medicine and Surgery, University of Missouri-Columbia, Columbia, Missouri; ²Research Service, Harry S. Truman Memorial Veterans' Hospital, Columbia, Missouri; ³Molecular Biology Program, University of Missouri-Columbia, Columbia, Missouri; ⁴Department of Biochemistry, University of Missouri-Columbia, Columbia, Missouri; ⁵Department of Chemistry, University of Missouri-Columbia, Columbia, Missouri; ⁶Department of Internal Medicine, University of Missouri-Columbia, Columbia, Missouri; ⁷Department of Radiology, University of Missouri-Columbia, Columbia, Missouri; and ⁸Nuclear Science and Engineering Institute, University of Missouri-Columbia, Columbia, Missouri

The *bcl-2* gene is overexpressed in non-Hodgkin's lymphoma (NHL), such as small lymphocytic lymphoma (SLL), and many other cancers. Noninvasive imaging of *bcl-2* expression has the potential to identify patients at risk for relapse or treatment failure. The purpose of this study was to synthesize and evaluate radiolabeled peptide nucleic acid (PNA)-peptide conjugates targeting *bcl-2* gene expression. An ^{111}In -labeled PNA complementary to the translational start site of *bcl-2* messenger RNA was attached to Tyr³-octreotide for somatostatin receptor-mediated intracellular delivery. **Methods:** DOTA-anti-*bcl-2*-PNA-Tyr³-octreotate (**1**) and 3 control conjugates (DOTA-nonsense-PNA-Tyr³-octreotate (**2**), DOTA-anti-*bcl-2*-PNA-Ala[3,4,5,6]-substituted congener (**3**), and DOTA-Tyr³-octreotate (**4**) [DOTA is 1,4,7,10-tetraazacyclododecane-*N,N',N'',N'''*-tetraacetic acid]) were synthesized by standard solid-phase 9-fluorenylmethoxycarbonyl (Fmoc) chemistry. In vitro studies were performed in Mec-1 SLL cells, which express both *bcl-2* messenger RNA and somatostatin receptors. Biodistributions and microSPECT/CT studies were performed in Mec-1-bearing SCID (severe combined immunodeficiency) mice, a new animal model of human SLL. **Results:** ^{111}In -Labeled conjugate **1** was taken up by Mec-1 cells through a somatostatin receptor-mediated mechanism. Biodistribution studies showed specific tumor uptake of conjugate **1**, the somatostatin analog **4**, and the PNA nonsense conjugate **2**, but not of the mutant peptide conjugate **3**. Mec-1 tumors could be detected by microSPECT/CT using ^{111}In -labeled DOTA-Tyr³-octreotate (**4**) and the targeted anti-*bcl-2* conjugate (**1**), but not using the 2 negative control conjugates **2** and **3**. **Conclusion:** A new ^{111}In -labeled antisense PNA-peptide conjugate demonstrated proof of principle for molecular imaging of *bcl-2* expression in a new mouse model of human SLL. This imaging agent may be useful for identifying NHL patients at risk for relapse and conventional treatment failure.

Key Words: *bcl-2*; peptide nucleic acid; somatostatin receptor; microSPECT/CT; non-Hodgkin's lymphoma

J Nucl Med 2008; **49**:430–438

DOI: 10.2967/jnmed.107.045138

The *B-cell lymphoma/leukemia-2* gene (*bcl-2*) is a human proto-oncogene discovered by Croce and coworkers (1). The *bcl-2* gene product is a dominant anti-apoptotic protein. Therefore, overexpression of *bcl-2* is frequently associated with higher relapse rates, shorter disease-free intervals, and poor survival in patients with aggressive B-cell lymphoma (2,3). Furthermore, *bcl-2* expression in tumor cells confers resistance to radiotherapy (4,5) and chemotherapy (6,7).

Small lymphocytic lymphoma/chronic lymphocytic leukemia (SLL/CLL) is one of the most common adult lymphoid malignancies in western countries (8) and is currently incurable (9). The aberrant expression of *bcl-2* has been detected in cells taken from SLL patients (10–12), making *bcl-2* a potential prognostic marker in SLL. Faderl et al. (13) compared the 5-y survival rate for patients with high and low levels of *bcl-2* expression. Patients with high *bcl-2* levels had 30% survival in that study, whereas a 70% survival rate was observed for the patients with low *bcl-2* expression.

Furthermore, downregulation of *bcl-2* expression has become a potential new treatment modality. Olimersen sodium (Bcl-2 antisense oligonucleotide, G3139, Genasense; Genta Inc.) is a phosphorothioate oligonucleotide complementary to the first 6 codons of the open reading frame of *bcl-2* messenger RNA (mRNA). This oligonucleotide activates degradation of *bcl-2* mRNA and inhibits protein synthesis (14). Preclinical studies have demonstrated that SLL cells treated with olimersen can augment

Received Jul. 10, 2007; revision accepted Nov. 12, 2007.

For correspondence or reprints contact: Michael R. Lewis, PhD, Department of Veterinary Medicine and Surgery, College of Veterinary Medicine, 900 E. Campus Dr., University of Missouri-Columbia, Columbia, MO 65211.

E-mail: LewisMic@missouri.edu

COPYRIGHT © 2008 by the Society of Nuclear Medicine, Inc.

response to both chemotherapy and rituximab (15,16). In a phase I/II multicenter study of G3139 in patients with advanced SLL, O'Brien et al. (17) reported that 8% of patients achieved partial responses and some other evidence of antitumor activity. Other studies also have been done to test the efficacy of oblimersen in other forms of non-Hodgkin's lymphoma (NHL) (18), multiple myeloma, and malignant melanomas (19). Therefore, bcl-2 antisense therapy constitutes a promising new treatment for malignant tumors (20).

Peptide nucleic acid (PNA) is a DNA-like molecule (21) composed of repeating *N*-(2-aminoethyl)-glycine units, to which the nucleobases are linked by methylene carbonyl groups. Relative to DNA and RNA oligonucleotides, these modifications increase the flexibility and binding affinity of PNA to complementary DNA or mRNA. PNAs have been shown to enhance nucleic acid specificity and inhibit protein expression (22,23). However, the major disadvantage of PNA is its poor cellular uptake. This problem can be circumvented by conjugating PNAs to cell-penetrating peptides (24) or receptor-avid peptides (25) for molecular imaging. Wickstrom and colleagues reported a series of receptor-targeted PNA-peptide chimeras labeled with 99m Tc or 64 Cu (26–28) for imaging oncogene mRNAs in breast cancer. Sun et al. (29) demonstrated that a 4-lysine tail is sufficient to deliver 64 Cu-labeled PNA for imaging of unr mRNA.

We previously reported that a cell-penetrating PTD-4-anti-*bcl-2*-PNA conjugate bound to *bcl-2* mRNA with high specificity and thermodynamic stability in cell-free systems (30). Although the PTD-4 peptide efficiently delivered the PNA into the correct intracellular compartments for mRNA targeting (24), the conjugate had no effect on *bcl-2* protein synthesis, suggesting a lack of antisense activity. In the present studies, we explored the strategy of somatostatin receptor-specific delivery of anti-*bcl-2*-PNA, to increase specific tumor uptake and antisense targeting. Tyr³-octreotate, a somatostatin analog, has been conjugated to anti-*n-myc*-PNA and shown to cause downregulation of *bcl-2* protein in IMR32 neuroblastoma cells (25). Because 84% of NHLs overexpress somatostatin receptors (31,32), we conjugated anti-*bcl-2*-PNA to Tyr³-octreotate and 1,4,7,10-tetraazacyclododecane-*N,N',N'',N'''*-tetraacetic acid (DOTA) for radiometal labeling. This conjugate, as well as nonsense PNA, alanine[3,4,5,6]-substituted congener peptide, and Tyr³-octreotate only conjugates, were labeled with 111 In and evaluated for receptor and mRNA binding, as well as SLL cell uptake, internalization, and retention. Finally, biodistribution and microSPECT/CT studies of the 4 conjugates were performed in a new SCID (severe combined immunodeficiency) mouse model of SLL.

MATERIALS AND METHODS

General

PNA-peptide synthesis reagents were high-performance liquid chromatography (HPLC) grade or peptide synthesis grade. Mass spectrometry (MS) was performed on a TSQ7000 mass spectrometer

(Thermo Finnigan) equipped with a NovaPak (Waters) C₁₈ column (5 μ m, 3.9 \times 300 mm). Reversed-phase HPLC (RP-HPLC) was performed on a Waters 626 chromatograph and a Phenomenex Jupiter C₁₈ column (5 μ m, 4.6 \times 250 mm). A gradient of 0%–50% solvent B (solvent A, 0.1% trifluoroacetic acid [TFA]/H₂O; solvent B, 0.1% TFA/acetonitrile) over 30 min at a flow rate of 1.0 mL/min was used.

111 InCl₃ was purchased from Mallinckrodt. Thin-layer chromatography (TLC) plates were developed with methanol/10% ammonium acetate (7:3, v/v), and radio-TLC detection was accomplished using a Bioscan AR-2000 TLC Imaging Scanner. Mec-1 cells were obtained from Dr. Charles W. Caldwell (Department of Pathology and Anatomical Sciences, University of Missouri-Columbia). Suspension cultures of cells were maintained in exponential growth phase in minimal essential medium (MEM; Invitrogen), supplemented with 10% fetal bovine serum, 2 mM L-glutamine, and 48 μ g/mL gentamycin, at 37°C and 5% CO₂. C.B-17/IcrHsd-Prkd SCID mice (4–6 wk of age) were obtained from Harlan Sprague-Dawley.

Synthesis of DOTA-PNA-Peptide Conjugates

DOTA-Tyr³-octreotate was synthesized on an Advanced Chemtech 396- Ω multiple synthesizer, using standard Fmoc chemistry. Peptidyl-resins without conjugated DOTA were transferred to a manual reaction vessel (Chemglass Inc.), where PNA synthesis was performed using modifications of methods described previously (24). DOTA was coupled at the end of synthesis using DOTA tris-*tert*-butyl ester. The conjugates were deprotected and detached from the resin by treatment for 4 h with TFA (87.5%) and 2.5% of each of the following scavengers: *m*-cresol, H₂O, phenol, thioanisole, 1,2-ethanedithiol, and triisopropylsilane. Precipitation and multiple washing with diethyl ether gave the final conjugates, which were analyzed by liquid chromatography-electrospray ionization–mass spectrometry (LC-ESI-MS).

Disulfide cyclization was accomplished by dimethyl sulfoxide (DMSO) oxidation of crude conjugates. Typically, the crude product, at a concentration of approximately 5 mg/mL, was dissolved and mixed overnight with DMSO/H₂O/CH₃CN (50:25:25). Each compound was purified by semipreparative RP-HPLC, using a stepwise gradient of 0%–20% solvent B in 10 min and 20%–40% solvent B in 60 min. Fractions corresponding to the desired products were pooled, lyophilized and analyzed by LC-ESI-MS.

111 In Labeling of Conjugates

Representative conditions for labeling DOTA-PNA-peptide conjugates with 111 In are given here. To 185 MBq of 111 In in 550–600 μ L of 0.2 M ammonium acetate, pH 5.0, containing approximately 1 mg/mL of gentisic acid and 0.1% Tween-80, was added 100 μ g of DOTA-PNA-peptide conjugates in 120–200 μ L of H₂O. The reaction mixture was incubated at 90°C for 30 min, with continuous mixing. Then an aliquot of 10 mM DTPA, pH 6.0, was added to a final DTPA concentration of 1 mM, and the reaction mixture was vortexed and incubated at room temperature for 5 min. The radiolabeled conjugates were purified by RP-HPLC as described. Purified fractions were concentrated to remove organic solvents. Then 5–10 mg of gentisic acid was added, the pH was adjusted to 5.0 with 0.1 M NaOH, 0.1% Tween-80 was added, and the solution was diluted with normal saline for injection.

DOTA-Tyr³-octreotate was labeled with 111 In as follows: 37 MBq of 111 InCl₃ in 150 μ L of 30 mM sodium acetate/25 mM sodium ascorbate, pH 5.0, was incubated with 1 μ g of DOTA-Tyr³-octreotate at 99°C for 30 min. Radiometal incorporation and

radiochemical purity (typically >98%) were determined by radio-TLC. The radiolabeled peptide was diluted with normal saline for injection without further purification.

In Vitro Binding Assay

The 50% inhibitory concentration (IC_{50}) values of ^{nat}In -DOTA-Tyr³-octreotate versus ^{111}In -DOTA-Tyr³-octreotate and ^{111}In -DOTA-anti-*bcl-2*-PNA-Tyr³-octreotate were determined by a competitive displacement assay in Mec-1 cell suspensions. Briefly, 2×10^6 cells in 200 μL of serum-free MEM were incubated at 37°C for 2 h in the presence of 7.4 kBq of ^{111}In -DOTA-Tyr³-octreotate or ^{111}In -DOTA-anti-*bcl-2*-PNA-Tyr³-octreotate and increasing concentrations of ^{nat}In -DOTA-Tyr³-octreotate. IC_{50} values were calculated by using Graftit software (Erithacus Software Ltd., U.K.).

Cell Uptake, Blocking, Efflux, and Internalization Studies

Aliquots of 37 kBq of the ^{111}In -labeled conjugates were added to 1×10^7 Mec-1 cells in 5 mL of MEM. During incubation at 37°C and 5% CO₂, triplicate aliquots were removed at various time points from 1 min to 4 h. Cells were isolated by centrifugation and counted separately from supernatant to determine the percentage uptake of radiopharmaceutical. For blocking experiments, 50 μg of unlabeled DOTA-Tyr³-octreotate was added simultaneously with the radiopharmaceuticals.

For internalization studies, radiopharmaceutical uptake was performed as described. The isolated cell pellet was washed with 0.2 M acetic acid/0.5 M NaCl, pH 2.5, to remove surface-bound radioactivity at each time point. Aliquots of the cells were counted separately from combined supernatants to determine the percentage internalization.

For efflux studies, radiopharmaceutical uptake was performed as described for 2 h at 37°C and 5% CO₂. Then cells were isolated by centrifugation, washed with fresh medium to remove residual radioactivity, and resuspended in fresh medium. Efflux of ^{111}In from the cells was measured at subsequent time points from 1 min to 4 h, after isolating aliquots of the cells and counting them separately from the supernatant, as described earlier.

Western Blot Analysis

Mec-1 cells (5×10^5 cells in 1 mL) were incubated with 2 μg of unlabeled PNA-peptide conjugates for 48 h. Then, cells were harvested, and whole cell lysates were electrophoresed on 12.5% sodium dodecyl sulfate polyacrylamide gel electrophoresis (SDS-PAGE) followed by electrical transferring of proteins onto nitrocellulose membranes. After blocking with 5% nonfat dry milk, 0.1% Tween-20, and phosphate-buffered saline, the membranes were incubated with *bcl-2* antibody (Santa Cruz Biotechnology) at a 1:1,000 dilution, followed by a secondary antimouse antibody conjugated with horseradish peroxidase (Jackson ImmunoResearch Laboratories) at a 1:20,000 dilution. Relative amounts of protein expression were determined by enhanced chemiluminescence and normalized to tubulin expression (26).

Biodistribution Studies

All animal experiments were conducted in compliance with the guidelines established by the Animal Care and Use Committee of the University of Missouri-Columbia and the Harry S. Truman Memorial Veterans' Hospital Subcommittee for Animal Studies. SCID mice were implanted subcutaneously in the hind flank with 1×10^7 Mec-1 cells in 0.1 mL of phosphate-buffered saline/Matrigel (BD Biosciences) (1:3). Four to 5 wk after tumor implantation, when tumors had grown to 100–400 mg, mice were

injected intravenously via the tail vein with 0.37 MBq of ^{111}In -labeled conjugates in 100 μL of normal saline. Biodistributions were obtained at 1, 4, 24, and 48 h after injection for ^{111}In -DOTA-PNA-peptide conjugates and at 1, 4, and 24 h for ^{111}In -DOTA-Tyr³-octreotate. Tissues harvested included blood, lung, liver, spleen, kidney, muscle, fat, heart, bone, bladder, stomach, small intestine, large intestine, and tumor. When possible, excess blood from the tissues was removed by absorbent paper. Tissues then were weighed and counted with a standard of the injected dose, such that decay-corrected uptakes were calculated as the percentage injected dose per gram of tissue (%ID/g) and the percentage injected dose per organ (%ID/organ).

Excretion Studies

SCID mice were injected intravenously with ^{111}In -DOTA-PNA-peptide conjugates as described earlier. Urine and feces were collected separately at 1, 4, 24, and 48 h after injection. Radioactivity was counted in the γ -counter with a standard of the injected dose, and the %ID for each sample was calculated.

Statistical Analysis

To compare the uptake of the organs at different time points of each compound, or the radioactivity accumulation in the same organ between different conjugates, a Student *t* test was performed. Differences at the 95% confidence level ($P < 0.05$) were considered significant.

MicroSPECT/CT

MicroSPECT/CT was performed using a Micro-CAT II SPECT/CT (Siemens Medical Solutions, Inc.) unit equipped with 2-mm pinhole collimators, with a magnification factor of 2.25. Mec-1-bearing SCID mice were injected with 4.4–21.1 MBq of ^{111}In -DOTA-anti-*bcl-2*-PNA-Tyr³-octreotate, ^{111}In -DOTA-anti-*bcl-2*-PNA-Ala[3,4,5,6], ^{111}In -DOTA-nonsense-PNA-Tyr³-octreotate, or 74 MBq of ^{111}In -DOTA-Tyr³-octreotate. Mice were imaged at 1 h after injection of ^{111}In -DOTA-Tyr³-octreotate and 1, 4, 24, and 48 h after injection of ^{111}In -DOTA-PNA-peptide conjugates. Energy-discriminating windows of 20% were used over the dual photopeaks of ^{111}In . SPECT scans were performed at 60 projections over 360°. Volumetric SPECT data were generated using a 3-dimensional ordered-subsets expectation maximization (OSEM) algorithm with geometric misalignment corrections. Twelve iterations and 4 subsets were used for SPECT image reconstruction. Concurrent microCT whole-body images were performed for anatomic coregistration with SPECT data. Reconstructed data from SPECT and CT were visualized and coregistered using AMIRA 3.1 (TGS, Mercury Computer Systems).

RESULTS

Synthesis of DOTA-PNA-Peptide Conjugates

A PNA-peptide conjugate, DOTA-anti-*bcl-2*-PNA-Tyr³-octreotate, specifically targeting *bcl-2* mRNA via somatostatin receptor-mediated delivery, was prepared using standard solid-phase Fmoc chemistry. The conjugate was purified by preparative RP-HPLC and characterized by LC-MS (m/z: calculated, 5,193.2; observed, 5,193.9). We also prepared a PNA mismatch control, DOTA-nonsense PNA-Tyr³-octreotate (m/z: calculated, 5,173.3; observed, 5,176.8), as well as a peptide mismatch control, DOTA-anti-*bcl-2*-PNA-Ala[3,4,5,6] (m/z: calculated, 4,898.9;

observed, 4,901.1), and peptide-only control, DOTA-Tyr³-octreotide. The structures of the conjugates are shown in Figure 1.

¹¹¹In Labeling

All conjugates were labeled with ¹¹¹In, using the conditions described earlier. The labeling efficiencies of DOTA-PNA-peptide conjugates were 40%–70%, and nearly 100% labeling was achieved for DOTA-Tyr³-octreotide. After purification, the radiochemical purity of ¹¹¹In-DOTA-PNA-peptide conjugates was nearly 100%, as radio-RP-HPLC gave single peaks at retention times of 20–23 min.

In Vitro Binding Assay

Under the experimental conditions described earlier, the IC₅₀ of ^{nat}In-DOTA-Tyr³-octreotide versus ¹¹¹In-DOTA-Tyr³-octreotide was 3.88 ± 0.43 nM, statistically equal to the previously reported value (33). The IC₅₀ of ^{nat}In-DOTA-Tyr³-octreotide versus ¹¹¹In-DOTA-anti-*bcl-2*-PNA-Tyr³-octreotide was approximately a factor of 2 different at 9 ± 3 nM (Fig. 2). Conjugation of PNA to the peptide had no significant effect on the binding affinity for somatostatin receptor subtype 2.

Cell Uptake, Blocking, Internalization, and Efflux Studies

Figures 3, 4, and 5 showed the results of uptake, blocking, internalization, and efflux study of ¹¹¹In-DOTA-PNA-peptide conjugates in Mec-1 cells. Uptake of ¹¹¹In-DOTA-anti-*bcl-2*-PNA-Tyr³-octreotide increased from 2.3% at 1 min to 5.2% at 4 h of incubation. At 4 h, excess DOTA-Tyr³-octreotide blocked 86% of cell-associated radioactivity, demonstrating somatostatin receptor-mediated cell uptake. In addition, 81% of cell-associated ¹¹¹In-DOTA-anti-*bcl-2*-PNA-Tyr³-octreotide was internalized in

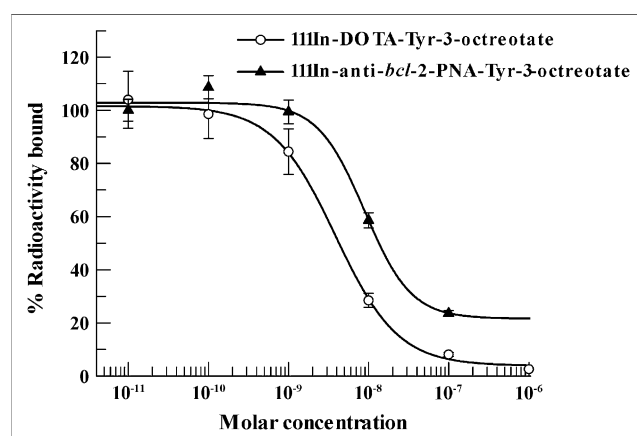


FIGURE 2. Somatostatin receptor binding of ¹¹¹In-DOTA-anti-*bcl-2*-PNA-Tyr³-octreotate and ¹¹¹In-DOTA-Tyr³-octreotate in Mec-1 cells.

Mec-1 cells at 4 h. Over a 4-h efflux study, 60% of radioactivity from ¹¹¹In-DOTA-anti-*bcl-2*-PNA-Tyr³-octreotate remained in the cells.

Under the same conditions, ¹¹¹In-DOTA-Tyr³-octreotate reached a maximum cell uptake of 2.6% at 4 h. As expected, cells incubated with excess DOTA-Tyr³-octreotate showed only 0.1%–0.4% cell uptake at all time points. The percentage of internalized ¹¹¹In-DOTA-Tyr³-octreotate increased with time and reached 66% at 4 h. Efflux studies showed that 69% of cell-associated radioactivity from ¹¹¹In-DOTA-Tyr³-octreotate remained at 4 h.

The uptake and internalization profiles of ¹¹¹In-DOTA-nonsense-PNA-Tyr³-octreotate in Mec-1 cells were similar to that of antisense conjugate. However, efflux studies showed that only 33% of the cell-associated radioactivity

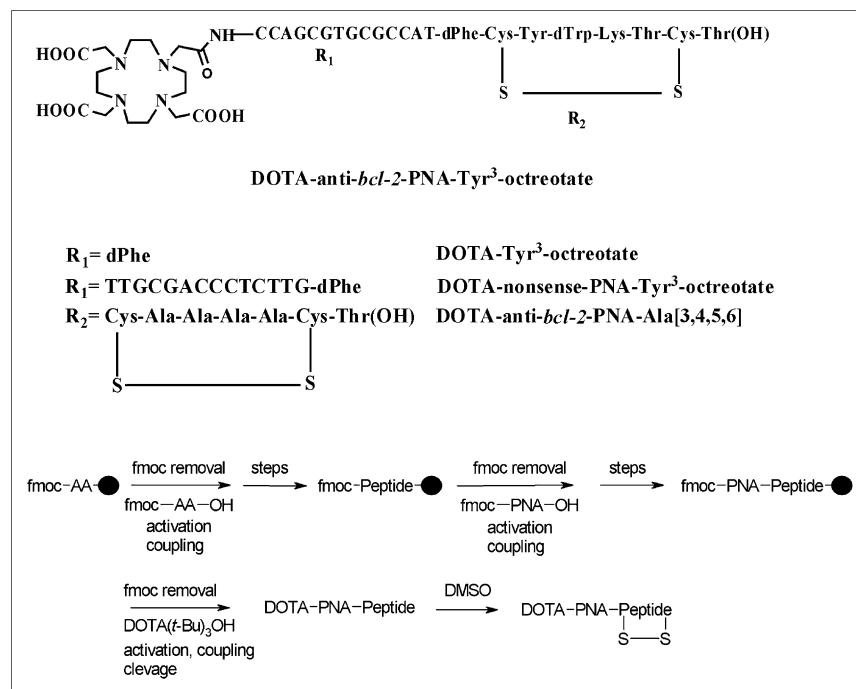


FIGURE 1. Structures and synthesis of DOTA-PNA-peptide conjugates.

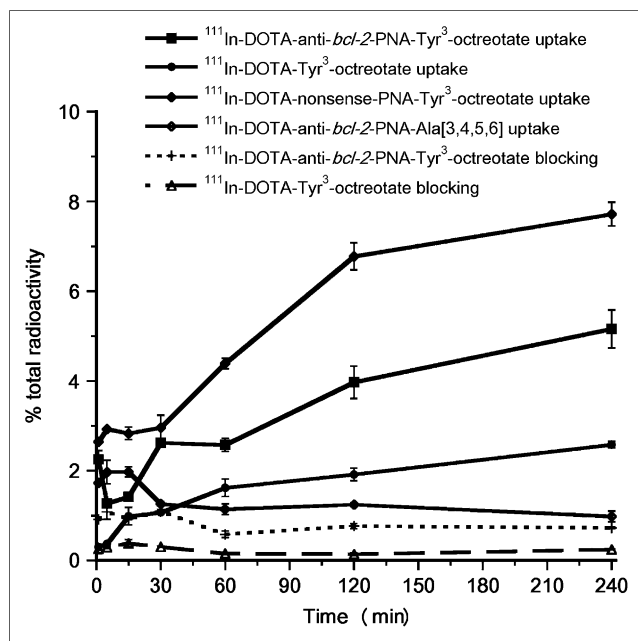


FIGURE 3. Uptake and blocking of ¹¹¹In-DOTA-PNA-peptide conjugates in Mec-1 cells ($n = 3$).

remained in the cells after 4 h, significantly lower ($P < 0.01$) than that of the antisense conjugate.

Because of the lack of targeted delivery, only 1%–1.5% of nonspecific binding was observed after incubation of ¹¹¹In-DOTA-anti-bcl-2-PNA-Ala[3,4,5,6] with Mec-1 cells for 4 h.

Western Blot Analysis

Western blot analysis (Fig. 6) showed a 51% inhibition of bcl-2 protein synthesis after treating Mec-1 cells with

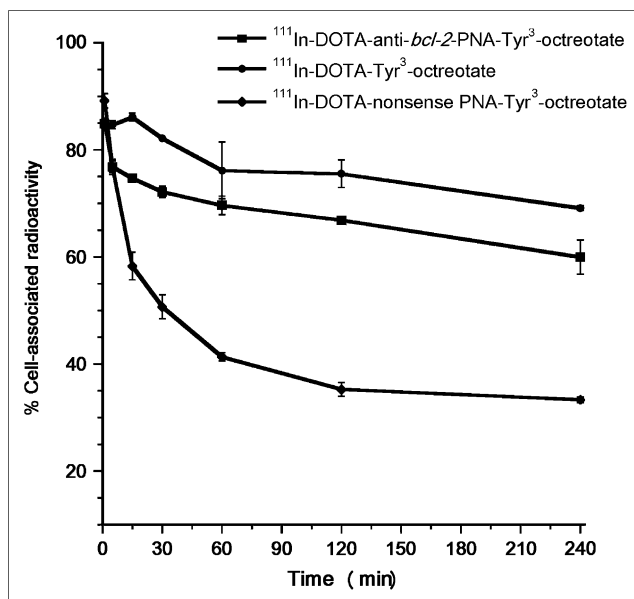


FIGURE 5. Efflux of ¹¹¹In-DOTA-PNA-peptide conjugates in Mec-1 cells ($n = 3$).

DOTA-anti-bcl-2-PNA-Tyr³-octreotate, but not with the 2 negative control compounds, DOTA-nonsense-PNA-Tyr³-octreotate and DOTA-anti-bcl-2-PNA-Ala[3,4,5,6]. The reduction in bcl-2 protein expression only after treatment with the conjugate containing targeted peptide and PNA sequences suggests that bcl-2 mRNA function had been perturbed by a specific antisense effect.

Biodistribution Studies

Biodistributions of ¹¹¹In-DOTA-PNA-peptide conjugates were obtained in a new mouse model of NHL, SCID mice bearing Mec-1 SLL xenografts. First, ¹¹¹In-DOTA-Tyr³-octreotate was evaluated for targeting somatostatin receptors. The biodistribution of ¹¹¹In-DOTA-Tyr³-octreotate is given in Table 1. This conjugate showed identical tumor uptake at 1 and 4 h after injection, 3.2 ± 0.8 %ID/g and 3.2 ± 0.9 %ID/g, respectively, and 46% of radioactivity was retained in the tumor after 48 h compared with that of 1 h. The uptake in other organs was low, except for metabolism and retention of the peptide in the kidneys.

The biodistribution of ¹¹¹In-DOTA-anti-bcl-2-PNA-Tyr³-octreotate is presented in Table 2. Tumor accumulation peaked at 4 h (1.4 ± 0.3 %ID/g), and 63% of radioactivity

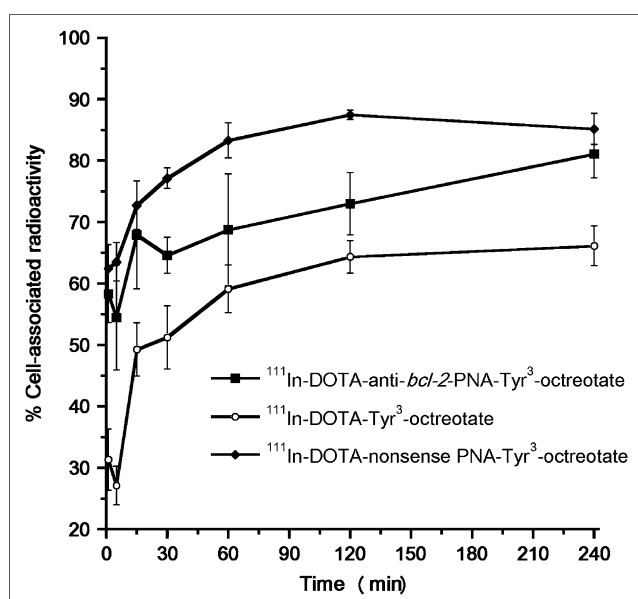


FIGURE 4. Internalization of ¹¹¹In-DOTA-PNA-peptide conjugates in Mec-1 cells ($n = 3$).

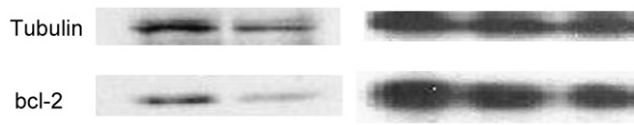


FIGURE 6. Western blot analysis of bcl-2 protein synthesis. Lane 1, untreated control; lane 2, cells treated with compound 1; lane 3, untreated control; lane 4, cells treated with compound 2; lane 5, cells treated with compound 3.

TABLE 1

Biodistribution of ^{111}In -DOTA-Tyr³-Octreotate in SCID Mice Bearing Mec-1 SLL Xenografts ($n = 5$)

Tissue	Biodistribution (%ID/g \pm SD)		
	1 h	4 h	24 h
Blood	0.31 \pm 0.07	0.06 \pm 0.01	0.02 \pm 0.003
Lung	8.27 \pm 1.88	6.87 \pm 0.54	4.12 \pm 0.84
Liver	0.32 \pm 0.07	0.29 \pm 0.06	0.20 \pm 0.04
Spleen	0.63 \pm 0.14	0.48 \pm 0.10	0.44 \pm 0.10
Kidney	11.4 \pm 1.70	11.0 \pm 1.46	6.39 \pm 0.73
Bladder	5.18 \pm 1.51	0.59 \pm 0.21	0.22 \pm 0.03
Muscle	0.04 \pm 0.01	0.02 \pm 0.002	0.01 \pm 0.001
Fat	0.08 \pm 0.026	0.03 \pm 0.008	0.01 \pm 0.003
Heart	0.26 \pm 0.03	0.12 \pm 0.02	0.07 \pm 0.02
Bone	0.52 \pm 0.10	0.57 \pm 0.10	0.22 \pm 0.05
Stomach	5.80 \pm 1.47	5.14 \pm 1.26	1.87 \pm 0.31
Small intestine	1.70 \pm 0.31	0.96 \pm 0.009	0.40 \pm 0.06
Large intestine	2.06 \pm 0.33	5.25 \pm 0.84	1.09 \pm 0.25
Tumor	3.24 \pm 0.77	3.24 \pm 0.85	1.49 \pm 0.29

was retained in the tumor at 48 h compared with that of 1 h. Kidney uptake was initially very high (130 ± 26 %ID/g at 4 h) but cleared by about a factor of 4 after 48 h (33 ± 6 %ID/g). Liver uptake was high at 1 h (13 ± 2 %ID/g) but dropped by a factor of 1.9 at 4 h and remained relatively constant out to 48 h. Blood uptake was initially low (2.6 ± 0.2 %ID/g at 1 h) and cleared relatively rapidly (0.19 ± 0.02 %ID/g at 48 h). Uptakes in other tissues were low at all time points. The tumor-to-muscle ratio increased from 4.12 to 7.30 from 1 to 48 h, suggesting specific tumor targeting.

The in vivo distribution of a PNA mismatch control, ^{111}In -DOTA-nonsense-PNA-Tyr³-octreotate, is shown in Table 3. Compared with the corresponding antisense conjugate, significantly lower tumor uptake was observed at 4 h (0.9 ± 0.2 %ID/g) and 24 h (0.8 ± 0.1 %ID/g). The kidney uptake of this conjugate was also very high initially (101 ± 23 %ID/g at 4 h) and cleared significantly slower

TABLE 3

Biodistribution of ^{111}In -DOTA-Nonsense-PNA-Tyr³-Octreotate in SCID Mice Bearing Mec-1 SLL Xenografts ($n = 5$)

Tissue	Biodistribution (%ID/g \pm SD)		
	4 h	24 h	48 h
Blood	1.27 \pm 0.30	0.25 \pm 0.02	0.09 \pm 0.01
Lung	1.23 \pm 0.21	0.77 \pm 0.15	0.51 \pm 0.07
Liver	6.34 \pm 1.19	5.74 \pm 0.59	5.61 \pm 0.70
Spleen	1.56 \pm 0.23	1.70 \pm 0.36	1.32 \pm 0.16
Kidney	100.7 \pm 23.3	76.1 \pm 9.82	53.3 \pm 6.06
Bladder	0.48 \pm 0.01	0.57 \pm 0.14	0.20 \pm 0.06
Muscle	0.13 \pm 0.03	0.08 \pm 0.01	0.07 \pm 0.01
Fat	0.14 \pm 0.02	0.17 \pm 0.04	0.07 \pm 0.01
Heart	0.50 \pm 0.08	0.26 \pm 0.01	0.19 \pm 0.01
Bone	0.30 \pm 0.03	0.24 \pm 0.05	0.18 \pm 0.05
Stomach	0.17 \pm 0.09	0.28 \pm 0.05	0.20 \pm 0.05
Small intestine	0.56 \pm 0.13	0.18 \pm 0.03	0.13 \pm 0.02
Large intestine	2.15 \pm 0.57	0.27 \pm 0.05	0.18 \pm 0.04
Tumor	0.89 \pm 0.21	0.75 \pm 0.13	0.57 \pm 0.08

than that of the antisense conjugate (53 ± 6 %ID/g at 48 h). The uptakes of the nonsense conjugate in other organs were similar to that of the antisense conjugate.

The biodistribution of a peptide mismatch control, ^{111}In -DOTA-anti-*bcl-2*-PNA-Ala[3,4,5,6], was also obtained in Mec-1 tumor-bearing mice. The results in Table 4 are indicative of a lack of in vivo targeting. Uptakes of this conjugate were low in all organs except the kidney, due to renal excretion.

Excretion studies showed that whole-body elimination of the 4 conjugates was dominated by renal clearance: 74 %ID by 24 h for ^{111}In -DOTA-Tyr³-octreotate and 88 %ID, 59 %ID, and 67 %ID by 48 h for ^{111}In -DOTA-anti-*bcl-2*-PNA-Tyr³-octreotate, ^{111}In -DOTA-nonsense PNA-Tyr³-octreotate, and ^{111}In -DOTA-anti-*bcl-2*-PNA-Ala[3,4,5,6], respectively.

TABLE 2

Biodistribution of ^{111}In -DOTA-Anti-*bcl-2*-PNA-Tyr³-Octreotate in SCID Mice Bearing Mec-1 SLL Xenografts ($n = 5$)

Tissue	Biodistribution (%ID/g \pm SD)			
	1 h	4 h	24 h	48 h
Blood	2.56 \pm 0.21	2.38 \pm 0.46	0.57 \pm 0.12	0.19 \pm 0.02
Lung	6.06 \pm 1.20	2.56 \pm 0.31	1.36 \pm 0.29	1.97 \pm 0.04
Liver	12.6 \pm 2.03	6.70 \pm 1.67	6.17 \pm 1.36	6.12 \pm 1.50
Spleen	2.75 \pm 0.51	1.34 \pm 0.04	1.36 \pm 0.28	1.05 \pm 0.06
Kidney	77.1 \pm 16.5	129.4 \pm 25.7	70.2 \pm 5.73	32.8 \pm 6.38
Bladder	1.71 \pm 0.93	1.34 \pm 0.29	0.84 \pm 0.18	0.71 \pm 0.18
Muscle	0.32 \pm 0.02	0.20 \pm 0.04	0.12 \pm 0.02	0.12 \pm 0.02
Fat	0.21 \pm 0.04	0.29 \pm 0.06	0.23 \pm 0.05	0.16 \pm 0.03
Heart	0.93 \pm 0.12	0.99 \pm 0.13	0.61 \pm 0.12	0.34 \pm 0.04
Bone	0.82 \pm 0.13	0.41 \pm 0.05	0.42 \pm 0.08	0.35 \pm 0.09
Stomach	2.12 \pm 0.70	2.33 \pm 0.79	1.02 \pm 0.18	0.51 \pm 0.14
Small intestine	1.24 \pm 0.19	0.79 \pm 0.21	0.32 \pm 0.04	0.24 \pm 0.04
Large intestine	1.19 \pm 0.12	2.26 \pm 0.47	0.48 \pm 0.07	0.41 \pm 0.10
Tumor	1.32 \pm 0.08	1.40 \pm 0.32	1.02 \pm 0.18	0.88 \pm 0.22

TABLE 4

Biodistribution of ^{111}In -DOTA-Anti-*bcl-2*-PNA-Ala[3,4,5,6] in SCID Mice Bearing Mec-1 SLL Xenografts ($n = 5$)

Tissue	Biodistribution (%ID/g \pm SD)		
	4 h	24 h	48 h
Blood	0.14 \pm 0.01	0.04 \pm 0.006	0.02 \pm 0.003
Lung	0.13 \pm 0.02	0.08 \pm 0.01	0.06 \pm 0.01
Liver	0.24 \pm 0.02	0.27 \pm 0.03	0.23 \pm 0.02
Spleen	0.09 \pm 0.02	0.11 \pm 0.01	0.12 \pm 0.005
Kidney	7.06 \pm 1.83	6.02 \pm 0.88	2.26 \pm 0.52
Bladder	0.06 \pm 0.01	0.17 \pm 0.03	0.10 \pm 0.02
Muscle	0.02 \pm 0.002	0.02 \pm 0.004	0.01 \pm 0.002
Fat	0.03 \pm 0.006	0.02 \pm 0.005	0.02 \pm 0.005
Heart	0.06 \pm 0.01	0.04 \pm 0.01	0.03 \pm 0.005
Bone	0.03 \pm 0.003	0.02 \pm 0.006	0.01 \pm 0.001
Stomach	0.10 \pm 0.002	0.03 \pm 0.007	0.02 \pm 0.001
Small intestine	0.06 \pm 0.005	0.04 \pm 0.004	0.02 \pm 0.003
Large intestine	0.19 \pm 0.01	0.05 \pm 0.01	0.02 \pm 0.005
Tumor	0.12 \pm 0.01	0.07 \pm 0.02	0.06 \pm 0.01

MicroSPECT/CT

The ability of the 4 conjugates to detect Mec-1 xenografts *in vivo* by microSPECT/CT was also investigated. For the purpose of direct comparison, images in Figure 7 were normalized to whole-body retention of radioactivity at the time of the highest tumor imaging contrast. As seen in Figure 7, Mec-1 tumors could be delineated at 1 h using ^{111}In -DOTA-Tyr³-octreotate. Low background activity was observed, except for high kidney uptake and urinary excretion, consistent with the biodistribution data. Tumors could be imaged by ^{111}In -DOTA-anti-*bcl-2*-PNA-Tyr³-octreotate as well, but only at 48 h, which may be due to renal clearance and a higher tumor-to-background ratio at later time points. High kidney uptake was observed in all images, as well as higher-than-expected liver uptake in some animals. Surprisingly, no tumor image was observed using ^{111}In -DOTA-nonsense-PNA-Tyr³-octreotate. Only kidneys and liver were seen at all time points. Injection

of ^{111}In -DOTA-anti-*bcl-2*-PNA-Ala[3,4,5,6] did not afford readily detectable SPECT images, because of the extremely rapid whole-body clearance of the nontargeted peptide conjugate.

DISCUSSION

Preclinical studies of *bcl-2* antisense therapy for B-cell malignancies have been designed to evaluate the potential of targeting clinically aggressive disease (34), and clinical trials with oblimersen are ongoing in patients with NHL (35), CLL/SLL (36), and multiple myeloma (37). Results from those studies are promising and support proof of the antisense principle. In the current study, we have developed an antisense imaging system with PNA-peptide conjugates targeting *bcl-2* mRNA and using Tyr³-octreotate for delivery to and internalization by tumor cell somatostatin receptors. This conjugate, as well as the peptide-only, PNA-mismatch, and peptide-mismatch conjugates, were labeled with ^{111}In and evaluated in Mec-1 cell and mouse models of SLL.

Receptor-targeted peptides have been shown to be efficient delivery vectors for PNA to target cellular oncogenes (25,26,38). Mier et al. have demonstrated that either oligodeoxynucleotides (ODNs) (39) or PNA against *bcl-2* mRNA (38) would not affect the binding affinity of Tyr³-octreotate to somatostatin receptors on rat cortex membranes. In the current studies, we demonstrated that the PNA-peptide conjugate showed similar binding affinity to the DOTA-conjugated peptide for somatostatin receptors on Mec-1 cells. Cell internalization and blocking studies further confirmed receptor-mediated uptake of these conjugates.

The hybridization properties of PNA are crucial for antisense targeting. Hybridization experiments have demonstrated that ^{90}Y -anti-*bcl-2*-PNA, conjugated with a cell-permeating peptide, PTD-4, was able to bind to immobilized *bcl-2* mRNA with high sensitivity, specificity, and stability (30). We also tested the hybridization of ^{111}In -DOTA-anti-*bcl-2*-PNA-Tyr³-octreotate and the PNA mismatch conjugate in this study (data not shown). Consistent with a

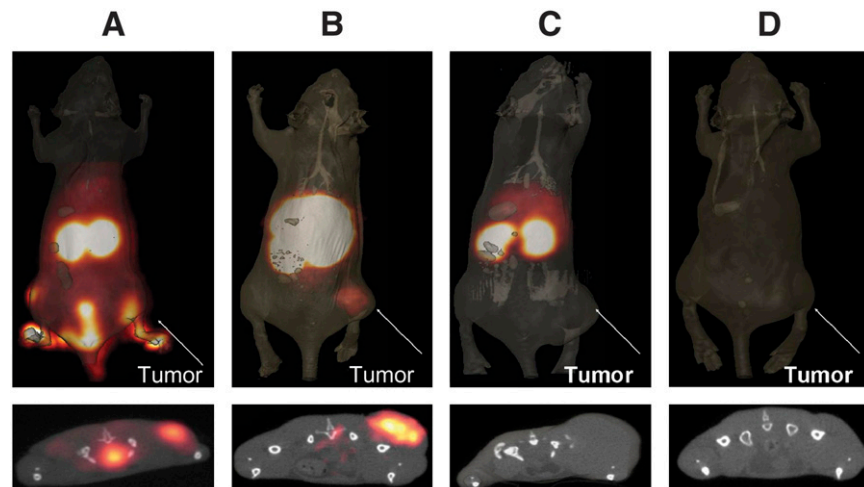


FIGURE 7. (Top) MicroSPECT/CT images of ^{111}In -DOTA-PNA-peptide conjugates in Mec-1-bearing SCID mice ($n = 3$). (A) ^{111}In -DOTA-Tyr³-octreotate (1 h). (B) ^{111}In -DOTA-anti-*bcl-2*-PNA-Tyr³-octreotate (48 h). (C) ^{111}In -DOTA-nonsense-PNA-Tyr³-octreotate (48 h). (D) ^{111}In -DOTA-anti-*bcl-2*-PNA-Ala[3,4,5,6] (48 h). (Bottom) Corresponding transaxial slices through the centers of the tumors.

previous report (30), the antisense conjugate showed binding affinity to *bcl-2* mRNA but not the PNA mismatch conjugate, which demonstrated the potential for antisense imaging. Western blot analysis also confirmed the protein synthesis inhibition activity of the *bcl-2* antisense PNA conjugate, after somatostatin receptor-mediated intracellular delivery.

The cell efflux study showed that nonsense conjugate washed out from the Mec-1 cells significantly faster than the antisense conjugate, which may be caused by the lack of mRNA targeting PNA sequence. Another experiment was also performed to better elucidate the mRNA targeting property of our antisense conjugate by using a *bcl-2* mRNA-deficient Ramos human lymphoma cell line (the ratio of the *bcl-2* mRNA level of Mec-1 cells to that of the Ramos cells was 3,822 determined by TaqMan real-time polymerase chain reaction). The efflux study results revealed 60% retention of antisense conjugate in Mec-1 cells compared with 15% in Ramos cells.

The biodistribution of ^{111}In -DOTA-anti-*bcl-2*-PNA-Tyr³-octreotate showed specific tumor uptake. The maximum tumor uptake ($1.4 \pm 0.3\% \text{ID/g}$) was comparable to that of ^{99m}Tc - (26,27) and ^{64}Cu -labeled (29) PNA-peptide compounds. ^{111}In -DOTA-nonsense-PNA-Tyr³-octreotate also showed tumor uptake, albeit significantly lower than that of the antisense conjugate at 4 and 24 h, which may be related to the lack of mRNA targeting. Both compounds showed high kidney uptake, consistent with that of the ^{64}Cu -labeled (29) PNA-peptide radiopharmaceuticals (143–280 %ID/g at 24 h). The ^{99m}Tc -PNA-peptide conjugates targeting *MYC* or *CCND1* (26,27) genes labeled with ^{99m}Tc showed lower kidney uptake (30–40 %ID/g at 4 h), possibly due to differences in radiometal metabolism. Although Sun et al. (29) observed the lower kidney uptake with ^{125}I than ^{64}Cu , the mechanisms of renal uptake of radiolabeled PNA-peptide conjugates are still unclear. In a pilot study in which lysine was used as the kidney-blocking agent, we observed that the kidney uptake of ^{111}In -DOTA-anti-*bcl-2*-PNA-Tyr³-octreotate was reduced by a factor of 3 at all time points.

Urinary excretion of ^{111}In -DOTA-anti-*bcl-2*-PNA-Tyr³-octreotate was relatively rapid from 4 to 48 h. Significantly lower urine excretion was observed for ^{111}In -DOTA-nonsense-PNA-Tyr³-octreotate ($P < 0.01$) at all time points. Metabolism studies showed that 95% of the antisense conjugate was intact in urine at 1 h after injection, whereas this value for the nonsense conjugate was 89% (significantly lower, $P < 0.05$). There was no significant change in these values out to 48 h after injection. The more hydrophilic metabolite associated with the nonsense conjugate likely contributed to the slower urinary clearance and higher kidney uptake at later time points.

In a pilot biodistribution study of the antisense conjugate in Ramos-bearing mice, a tumor uptake of 0.2% was observed compared with 1.3% in Mec-1 mice at 48 h, which also suggested a specific *bcl-2* mRNA targeting of this conjugate in Mec-1 tumors *in vivo*.

Imaging of Mec-1 tumors using ^{111}In -DOTA-Tyr³-octreotate and ^{111}In -DOTA-anti-*bcl-2*-PNA-Tyr³-octreotate was expected on the basis of cellular internalization and retention, as well as specific tumor uptake. As shown in Figure 7, the peptide-only conjugate was able to delineate tumors as early as 1 h. Tumors could be detected with the targeted antisense conjugate, but only at 48 h. This result may be partially due to the slow hybridization of PNA to the target mRNA (29). Another reason for prolongation of antisense imaging could be the high kidney uptake at earlier time points, which may have obscured tumor imaging when even modest backscatter smoothing was applied. The tumor-to-kidney ratio of this conjugate increased significantly from 4 to 48 h ($P < 0.02$). No significant difference ($P = 0.07$) in renal uptake was observed between 4 and 24 h. Tumors were not detected by imaging using the nonsense PNA conjugate, which contains the correct receptor-binding peptide. At 48 h, the tumor-to-kidney ratio of the targeted antisense conjugate was significantly higher ($P < 0.03$) than that of the nonsense conjugate. The slower kidney clearance and the lower tumor uptake of this compound, compared with the corresponding antisense conjugate, may have compromised imaging contrast such that tumors were not detected.

Although human SLL xenografts could be detected by our targeted antisense conjugate, the high kidney accumulation compromised image quality to some degree. To promote renal and hepatobiliary clearance, modified PNA monomers with neutral hydrophilic (serine, T_S) or negatively charged (aspartic acid, T_D) residues were synthesized (40) as substitutes for glycine at T¹⁴ in the PNA sequence. Those analogs are currently being studied *in vitro* and *in vivo*. Other strategies, such as using kidney-blocking agents or higher-sensitivity microPET, are also being evaluated to obtain optimal biodistribution and imaging results.

CONCLUSION

We developed a receptor-specific PNA-peptide conjugate for antisense imaging of *bcl-2* expression in SLL xenografts. A tetradecamer PNA sequence targeting *bcl-2* mRNA was conjugated at the *N*-terminus with DOTA, for radiometal labeling, and at the *C*-terminus with Tyr³-octreotate, for somatostatin receptor-mediated delivery. The ^{111}In -labeled conjugate showed specific receptor-mediated cell uptake and *bcl-2* mRNA binding in Mec-1 SLL cells. Mec-1 tumors in SCID mice were imaged using ^{111}In -DOTA-anti-*bcl-2*-PNA-Tyr³-octreotate, demonstrating the principle of antisense imaging in a new mouse model of human lymphoma.

ACKNOWLEDGMENTS

We thank Dr. Charles W. Caldwell for providing the Mec-1 cell line. We also thank Lisa Watkinson, Terry Carmack, and Tiffani Shelton for excellent technical assistance. This

work was supported by NIH grant CA103130 from the National Cancer Institute.

REFERENCES

- Tsujimoto Y, Cossman J, Jaffe E, Croce CM. Involvement of the *bcl-2* gene in human follicular lymphoma. *Science*. 1985;228:1440–1443.
- Hermine O, Haioun C, Lepage E, et al. Prognostic significance of *bcl-2* protein expression in aggressive non-Hodgkin's lymphoma. *Blood*. 1996;87:265–272.
- Hill ME, MacLennan KA, Cunningham DC, et al. Prognostic significance of BCL-2 expression and *bcl-2* major breakpoint region rearrangement in diffuse large cell non-Hodgkin's lymphoma: a British national lymphoma investigation study. *Blood*. 1996;88:1046–1051.
- Milner AE, Grand RJ, Vaughan ATM, Armitage RJ, Gregory CD. Differential effects of BCL-2 on survival and proliferation of human B-lymphoma cells following gamma-irradiation. *Oncogene*. 1997;15:1815–1822.
- Mirkovic N, Voehringer DW, Story MD, McConkey DJ, McDonnell TJ, Meyn RE. Resistance to radiation-induced apoptosis in Bcl-2-expressing cells is reversed by depleting cellular thiols. *Oncogene*. 1997;15:1461–1470.
- Miyashita T, Reed JC. *bcl-2* gene transfer increases relative resistance of S49.1 and WEHI7.2 lymphoid cells to cell death and DNA fragmentation induced by glucocorticoids and multiple chemotherapeutic drugs. *Cancer Res*. 1992;52:5407–5411.
- Miyashita T, Reed JC. Bcl-2 oncoprotein blocks chemotherapy-induced apoptosis in a human leukemia cell line. *Blood*. 1993;81:151–157.
- Jemal A, Murray T, Samuels A, Ghafoor A, Ward E, Thun MJ. Cancer statistics, 2003. *CA Cancer J Clin*. 2003;53:5–26.
- Mavromatis BH, Cheson BD. Novel therapies for chronic lymphocytic leukemia. *Blood Rev*. 2004;18:137–148.
- Lazaridou A, Miraxtzi C, Korantzis J, Eleftheriadis N, Christakis JI. Simultaneous detection of BCL-2 protein, trisomy 12, retinoblastoma and P53 monoallelic gene deletions in B-cell chronic lymphocytic leukemia by fluorescence in situ hybridization (FISH): relation to disease status. *Leuk Lymphoma*. 2000;36:503–512.
- Pepper C, Bentley P, Hoy T. Regulation of clinical chemoresistance by *bcl-2* and *bax* oncoproteins in B-cell chronic lymphocytic leukemia. *Br J Haematol*. 1996;95:513–517.
- Veis DJ, Sorenson CM, Shutter JR, Korsmeyer SJ. Bcl-2-deficient mice demonstrate fulminant lymphoid apoptosis, polycystic kidneys, and hypopigmented hair. *Cell*. 1993;75:229–240.
- Faderl S, Keating MJ, Do K-A, et al. Expression profile of 11 proteins and their prognostic significance in patients with chronic lymphocytic leukemia (CLL). *Leukemia*. 2002;16:1045–1052.
- Klasa RJ, Gillum AM, Klem RE, Frankel SR. Oblimersen Bcl-2- antisense: facilitating apoptosis in anticancer treatment. 2002;12:193–213.
- Pepper C, Thomas A, Hoy T, Cotter F, Bentley P. Antisense-mediated suppression of Bcl-2 highlights its pivotal role in failed apoptosis in B-cell chronic lymphocytic leukaemia. *Br J Haematol*. 1999;107:611–615.
- Auer RL, Corbo M, Fegan CD, Frankel SR, Cotter FE. Bcl-2 antisense (Genasense) induces apoptosis and potentiates activity of both cytotoxic chemotherapy and rituximab in primary CLL cells [abstract]. *Blood*. 2001;98:808a.
- O'Brien SM, Cunningham CC, Golenkov AK, Turkina AG, Novick SC, Rai KR. Phase I to II multicenter study of oblimersen sodium, a Bcl-2 antisense oligonucleotide, in patients with advanced chronic lymphocytic leukemia. *J Clin Oncol*. 2005;23:7697–7702.
- Webb A, Cunningham D, Cotter F, et al. *BCL-2* antisense therapy in patients with non-Hodgkin lymphoma. *Lancet*. 1997;349:1137–1141.
- Jansen B, Wacheck V, Heere-Ress E, et al. Chemosensitization of malignant melanoma by BCL2 antisense therapy. *Lancet*. 2000;356:1728–1733.
- Kim R, Tanabe K, Emi M, Uchida Y, Toge T. Potential roles of antisense therapy in the molecular targeting of genes involved in cancer. *Int J Oncol*. 2004;24:5–17.
- Nielsen PE, Egholm M, Berg RH, Buchardt O. Sequence-selective recognition of DNA by strand displacement with a thymine-substituted polyamide. *Science*. 1991;254:1497–1500.
- Doyle DF, Braasch DA, Simmons CG, Janowski BA, Corey DR. Inhibition of gene expression inside cells by peptide nucleic acids: effect of mRNA target sequence, mismatched bases, and PNA length. *Biochemistry*. 2001;40:53–64.
- Stock RP, Olvera A, Sanchez R, et al. Inhibition of gene expression in *Entamoeba histolytica* with antisense peptide nucleic acid oligomers. *Nat Biotechnol*. 2001;19:231–234.
- Gallazzi F, Wang Y, Jia F, et al. Synthesis of radiometal-labeled and fluorescent cell-permeating peptide-PNA conjugates for targeting the bcl-2 proto-oncogene. *Bioconjug Chem*. 2003;14:1083–1095.
- Sun L, Fuselier JA, Murphy WA, Coy DH. Antisense peptide nucleic acids conjugated to somatostatin analogs and targeted at the n-myc oncogene display enhanced cytotoxicity to human neuroblastoma IMR32 cells expressing somatostatin receptors. *Peptides*. 2002;23:1557–1565.
- Tian X, Aruva MR, Qin W, et al. External imaging of CCND1 cancer gene activity in experimental human breast cancer xenografts with ^{99m}Tc -peptide-peptide nucleic acid-peptide chimeras. *J Nucl Med*. 2004;45:2070–2082.
- Tian X, Aruva MR, Qin W, et al. Noninvasive molecular imaging of MYC mRNA expression in human breast cancer xenografts with a ^{99m}Tc -peptide-peptide nucleic acid-peptide chimera. *Bioconjug Chem*. 2005;16:70–79.
- Chakrabarti A, Aruva MR, Sajankila SP, Thakur ML, Wickstrom E. Synthesis of novel peptide nucleic acid-peptide chimera for non-invasive imaging of cancer. *Nucleosides Nucleotides Nucleic Acids*. 2005;24:409–414.
- Sun X, Fang H, Li X, Rossin R, Welch MJ, Taylor JS. MicroPET imaging of MCF-7 tumors in mice via unr mRNA-targeted peptide nucleic acids. *Bioconjug Chem*. 2005;16:294–305.
- Lewis MR, Jia F, Gallazzi F, et al. Radiometal-labeled peptide-PNA conjugates for targeting bcl-2 expression: preparation, characterization, and in vitro mRNA binding. *Bioconjug Chem*. 2002;13:1176–1180.
- Lugtenburg PJ, Löwenberg B, Valkema R, et al. Somatostatin receptor scintigraphy in the initial staging of low-grade non-Hodgkin's lymphomas. *J Nucl Med*. 2001;42:222–229.
- Reubi JC, Waser B, van Hagen M, et al. *In vitro* and *in vivo* detection of somatostatin receptors in human malignant lymphomas. *Int J Cancer*. 1992;50:895–900.
- de Jong M, Breeman WA, Bakker WH, et al. Comparison of ^{111}In -labeled somatostatin analogues for tumor scintigraphy and radionuclide therapy. *Cancer Res*. 1998;58:437–441.
- Chanan-Khan A. Bcl-2 antisense therapy in B-cell malignancies. *Blood Rev*. 2005;19:213–221.
- Waters JS, Webb A, Cunningham D, et al. Phase I clinical and pharmacokinetic study of bcl-2 antisense oligonucleotide therapy in patients with non-Hodgkin's lymphoma. *J Clin Oncol*. 2000;18:1812–1823.
- Rai KR, O'Brien S, Cunningham C, et al. Genasense (Bcl-2 antisense) monotherapy in patients with relapsed or refractory chronic lymphocytic leukemia: phase 1 and 2 results [abstract]. *Blood*. 2002;100:384a.
- Badros AZ, Ratterree B, Natt S, et al. Phase I/II trial of oblimersen sodium (G3139), dexamethasone (Dex) and thalidomide (Thal) in patients with relapsed multiple myeloma [abstract]. *Blood*. 2003;102:684a.
- Mier W, Eritja R, Mohammed A, Haberkorn U, Eisenhut M. Peptide-PNA conjugates: targeted transport of antisense therapeutics into tumors. *Angew Chem Int Ed Engl*. 2003;42:1968–1971.
- Mier W, Eritja R, Mohammed A, Haberkorn U, Eisenhut M. Preparation and evaluation of tumor-targeting peptide-oligonucleotide conjugates. *Bioconjug Chem*. 2000;11:855–860.
- Balaji BS, Gallazzi F, Jia F, Lewis MR. An efficient, convenient solid-phase synthesis of amino acid modified peptide nucleic acid monomers and oligomers. *Bioconjug Chem*. 2006;17:551–558.